

$b \rightarrow c$  HADRONIC DECAYS

JORGE L. RODRIGUEZ

*Department of Physics and Astronomy, University of Hawaii, 2505 Correa Road,  
Honolulu, Hawaii 96822, USA  
University of Hawaii preprint UH 511-892-98*

A review of current experimental results on exclusive hadronic decays of bottom mesons to a single or double charmed final state is presented. We concentrate on branching fraction measurements conducted at  $e^+e^-$  colliders at the  $\Upsilon(4S)$  and at the  $Z^0$  resonance. The experimental results reported are then used in tests of theoretical model predictions, the determination of the QCD parameters  $a_1$  and  $a_2/a_1$  and tests of factorization.

**1 Introduction**

In  $b \rightarrow c$  hadronic transitions the spectator processes dominate. Other processes, such as the exchange or annihilation channels are suppressed relative to the spectator processes through form-factor suppression<sup>1</sup>. Two classes of spectator processes are possible –internal and external spectator (See Fig. 1)– each defined by the quark-color arrangement of the final state. In the factorization approximation three classes of spectator decays can be identified. In Class I or Class II decays, the quark configuration of the final states, neglecting final-state rescattering, is possible only if the decay proceeds either through the external or internal diagram respectively. A third type of decay, Class III, the quark configuration of the final-states can be obtained via both diagrams.

In this article I will describe the latest experimental results on the following hadronic two-body decays of the  $B$  meson:

Class I	Class II	Class III
$B^0 \rightarrow D^{(*)+}(n\pi)^-$	$B^0 \rightarrow D^{(*)0}(n\pi)^0$	$B^- \rightarrow D^{(*)0}(n\pi)^-$
$B^0 \rightarrow D_J^+(n\pi)^-$		$B^- \rightarrow D_J^0(n\pi)^-$
$B^0 \rightarrow D^{(*)+}D_s^{(*)-}$		$B^- \rightarrow D^0 K^-$

concentrating on the experimental techniques employed in measurements of branching fractions. I will also discuss some of the more important theoretical implications including tests of factorization and determination of the QCD parameters  $a_1$  and  $a_2/a_1$ .

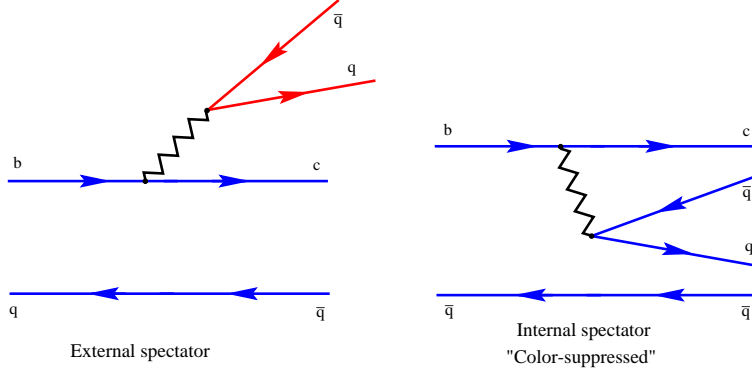


Figure 1: Tree level decay diagrams dominant in two-body hadronic decays of  $B$  mesons.

## 2 Experimental Programs

Except for the  $B \rightarrow J/\psi K$  decays, measurements of hadronic decay rates of the  $B$  meson to charm have been performed exclusively in  $e^+e^-$  experiments. Decay rate measurements are dominated by experiments conducted at  $B\bar{B}$  threshold while experiments at higher energy have provide information on  $b$  lifetimes and on higher mass hadrons e.g.,  $B_s$ ,  $\Lambda_b$  not accessible to experiments at  $B\bar{B}$  threshold. Recently, experiments at CERN have made contributions to measurement of exclusive decays with a measurements from OPAL on  $\bar{B}^0 \rightarrow D^{*+}\pi^-$  and ALEPH measurements of several  $B \rightarrow DD_s X, DD X$  and two-body  $D^{(*)}D_s^{(*)}$  decays. In the next section I will briefly describe the OPAL measurement as an example of the experimental method employed at the high energy  $e^+e^-$  experiments. I will then concentrate on recent measurements performed at CLEO II since they are the dominant contributors to measurements of exclusive hadronic decays of  $B_{d,u}$  mesons.

### 2.1 Measurement of the branching fraction of $\bar{B}^0 \rightarrow D^{*+}\pi^-$ at OPAL

The large sample of  $Z^0$  produced at LEP coupled with a reasonable partial width to  $b\bar{b}$  (6%) provides a significant number of  $B\bar{B}$  events to examine. Unfortunately the small branching fractions to any particular  $B$  decay mode and the large particle multiplicities involved present difficult obstacles in exclusive reconstruction of hadronic  $B$  decays. Given these obstacles OPAL has a new measurement of  $\bar{B}^0 \rightarrow D^{*+}\pi^-$  with their sample of  $1.2 \times 10^6$  hadronic  $Z^0$  decays.

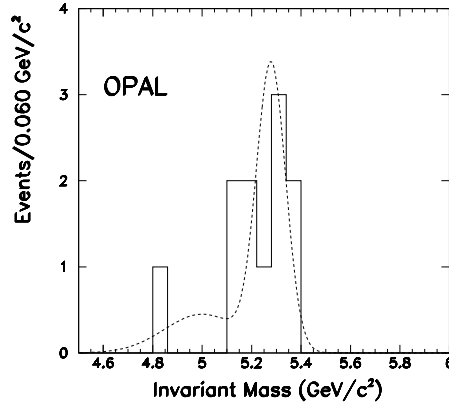


Figure 2: The invariant mass distribution of fully reconstructed  $B_d$  mesons at OPAL. The dashed curve is the fit to data. It is a sum of two Gaussians plus a straight line. The first Gaussian represents the signal the other the feed-down from the  $\bar{B}^0 \rightarrow D^{*+} \rho^-$  decays. The straight line models the combinatoric background.

The analysis<sup>6</sup> features a full reconstruction of the decay chain:<sup>a</sup>

$$B^0 \rightarrow D^{*+} \pi^-; \quad D^{*+} \rightarrow D^0 \pi^+; \quad D^0 \rightarrow K^- \pi^+$$

where charged tracks are combined to form candidate particles. Each track in the event is identified as either a kaon or pion depending primarily on its energy loss in the jet chamber. Additional requirements on track transverse momentum and impact parameter are imposed. The invariant mass of the  $K^- \pi^+$  combination is required to be within 90 MeV of the nominal  $D^0$  mass and the mass difference between the  $K^- \pi^+$  and  $(K^- \pi^+) \pi^+$  combination is required to be within 2 MeV/ $c^2$  of the known mass difference. The  $D^0$  and  $D^{*+}$  candidates are formed separately for each jet and are then combined with other tracks in the jet to form a  $B_d$  candidate. To reduce combinatorial backgrounds, a decay angle cut is imposed on the  $D^0$  candidates and a helicity angle cut is imposed on the angular distribution of the decay products of the  $D^{*+}$ .

The hard fragmentation of the  $b$  quark and its long lifetime are also exploited to reduce combinatorial background. The momentum of the  $B_d$  candidate is required to exceed 70% of the beam energy and the  $B_d$  and  $D^0$  decay vertices are required to be in the hemisphere centered around the  $B_d$  momentum vector.

---

<sup>a</sup>Charge-conjugate states are implied throughout this article

After application of the selection criteria, 11 events are observed in the mass region between 4.5 and 6.0 GeV/c<sup>2</sup>, see Fig. 2. To determine the event yield the  $m_B$  distribution is fit to two-Gaussians plus a straight line. The second Gaussian takes into account the feed-down from  $\bar{B}^0 \rightarrow D^{*+}\rho^-$  decays which have been miss-reconstructed as a  $\bar{B}^0 \rightarrow D^{*+}\pi^-$ . This background peaks below the  $B_d$  mass and is fixed in the fit to the value determined in a Monte Carlo simulation. Monte Carlo data is also used to determine the widths of both Gaussians. The fit yields  $8.1 \pm 2.9$  events for the  $\bar{B}^0 \rightarrow D^{*+}\pi^-$  and  $2.9 \pm 1.9$  for the  $\bar{B}^0 \rightarrow D^{*+}\rho^-$  mode at a mass of  $5.279 \pm 0.023$  GeV/c<sup>2</sup>. The branching fraction is estimated to be:

$$\mathcal{B}r(\bar{B}^0 \rightarrow D^{*+}\pi^-) = (1.0 \pm 0.4 \pm 0.1)\%$$

The Standard Model value for  $\Gamma_{bb}/\Gamma_{\text{had}} = 0.217$  and the  $B_d$  production fraction ( $f_{B_d} = 0.38$ ) are used<sup>6</sup>. This value is consistent with previous CLEO and ARGUS results<sup>7</sup> and with current CLEO II results<sup>8</sup>.

### 3 Measurements at $B\bar{B}$ Threshold

The large luminosity and clean environment typical at  $e^+e^-$  machines running at the  $B\bar{B}$  threshold provide very large samples of  $B\bar{B}$  events. For example, at CLEO the numbers of  $B\bar{B}$  events collected from 1994 through 1996 was  $3.1 \times 10^6$  while ARGUS whose physics runs ended in 1993, collected about 330,000  $B\bar{B}$  pairs.

The event topology at  $B\bar{B}$  threshold is somewhat different than at a machine running on the  $Z^0$  resonance. In particular, two characteristics differentiate the reconstruction technique from that employed in the higher energy environment. First, significantly larger backgrounds are encountered from continuum processes. At  $B\bar{B}$  threshold 3/4 of the total hadronic cross-section is from continuum events. Fortunately, this background is well behaved and can be accurately modeled by data taken below  $B\bar{B}$  threshold; nevertheless, techniques must be employed to reduce the contribution from these backgrounds. Secondly, the fact that the  $B$  mesons are produced nearly at rest is exploited to improve signal identification. Signal extraction is improved by replacing the energy of the reconstructed  $B$  meson with the energy of the beam which is typically known better by an order of magnitude than the reconstructed energy.

In the following sections I will discuss new results from CLEO using the complete CLEO II data sample which consists of  $3.1 fb^{-1}$  taken at the  $\Upsilon(4S)$ . A smaller sample of  $1.4 fb^{-1}$  taken just below the  $\Upsilon(4S)$  is also used to model the continuum background. These results have either been reported at conferences

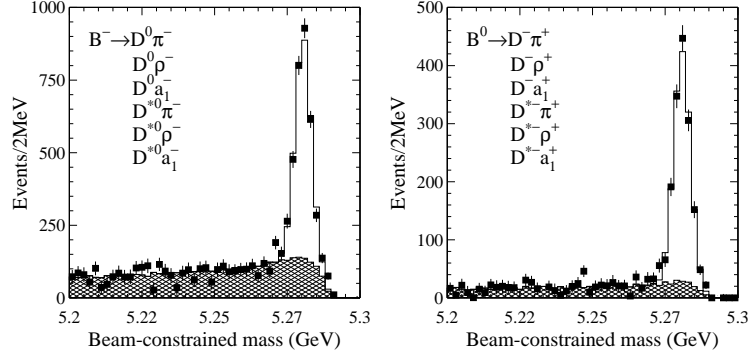


Figure 3: The continuum-subtracted beam-constrained mass distributions for twelve  $B \rightarrow D^{(*)}n\pi$  modes. The hatched histograms shows the  $B\bar{B}$  background spectrum, the open histograms is fit to data by the sum of a Gaussian of plus the  $B\bar{B}$  background distribution determined from Monte Carlo simulations. The data are the black squares with error bars.

or have been recently published. All of the  $B$  branching fractions presented in Tables 1,2 and 3 have been rescaled to the  $D^0, D^+, D^{*+}$  and  $D^{*0}$  branching fractions used in Ref. [8]. The  $D_s^{(*)}$  branching fractions used are taken from Ref. [9].

### 3.1 Full Reconstruction of $B \rightarrow D^{(*)}(n\pi)$ decays at CLEO

CLEO has recently updated their branching fraction measurements of 22 decay modes of the  $B_{d,u}$  mesons. These have been released as conference reports<sup>8,10</sup>. The analyses described here utilize the full reconstruction technique, similar to the method described in the previous section but optimized to exploit the kinematic properties unique to  $B\bar{B}$  production from the decay of the  $\Upsilon(4S)$ . Once again the goal is to maximize the number of  $B$  mesons by combining a selection of charged and neutral tracks into particle candidates which in turn are combined to reconstruct the  $B$  meson decay chain. The charmed candidates are formed from a selected sample of charged tracks and  $\pi^0$  in the following decay modes:

$$\begin{aligned} D^{*0} &\rightarrow D^0\pi^0 & D^{*+} &\rightarrow D^0\pi^+ \\ D^0 &\rightarrow K^-\pi^+, K^-\pi^+\pi^0, K^-\pi^+\pi^-\pi^+ & D^+ &\rightarrow K^-\pi^+\pi^+. \end{aligned}$$

Invariant mass cuts are applied to the  $D^0$  and  $D^-$  candidates and the  $D^*, D^0$  mass difference is used to select  $D^{*+}$  and  $D^{*0}$  candidates.

To reduce continuum background two quantities are used. The global event topology is exploited by cutting on the ratio of the 2<sup>nd</sup> to 1<sup>st</sup> Fox-Wolfram moment, selecting events above 0.5. Second, the sphericity angle  $\theta_f$

Table 1: Branching Fractions for  $B \rightarrow D^{(*)}(n\pi)^-$  Decay Modes<sup>23</sup>

Class I Decays		Class III Decays	
Mode	$\mathcal{Br}$ (%)	Mode	$\mathcal{Br}$ (%)
$D^+\pi^-$	$0.25 \pm 0.02 \pm 0.03$	$D^0\pi^-$	$0.47 \pm 0.03 \pm 0.04$
$D^{*+}\pi^-$ <sup>11</sup>	$0.27 \pm 0.01 \pm 0.02$	$D^{*0}\pi^-$ <sup>11</sup>	$0.40 \pm 0.03 \pm 0.04$
$D^+\rho^-$ <sup>12</sup>	$0.79 \pm 0.07 \pm 0.12$	$D^0\rho^-$ <sup>12</sup>	$0.92 \pm 0.08 \pm 0.08$
$D^{*+}\rho^-$ <sup>12</sup>	$0.73 \pm 0.06 \pm 0.08$	$D^{*0}\rho^-$ <sup>12</sup>	$1.28 \pm 0.13 \pm 0.14$
$D^+a_1^-$ <sup>13</sup>	$0.83 \pm 0.09 \pm 0.14$	$D^0a_1^-$ <sup>13</sup>	$0.89 \pm 0.10 \pm 0.11$
$D^{*+}a_1^-$ <sup>13</sup>	$1.16 \pm 0.12 \pm 0.16$	$D^{*0}a_1^-$ <sup>13</sup>	$1.60 \pm 0.25 \pm 0.24$
		$D_1^0\pi^-$	$0.12 \pm 0.02 \pm 0.03$
		$D_2^{*0}\pi^-$	$0.21 \pm 0.08 \pm 0.03$
		$D^0K^-$	$< 0.044$

is used. It too exploits the difference between the event topology of continuum and  $B\bar{B}$  events. The sphericity angle is defined as the angle between the sphericity axis for tracks which form the  $B$  candidate and the sphericity axis for the remaining tracks in the event. For real  $B$  events this angle is isotropic thus the  $|\cos\theta_f|$  quantity is distributed uniformly from 0 to 1. For continuum events this quantity populates the region near 1.0. By selecting candidates with  $|\cos\theta_f| \leq 0.8$  a considerable portion of the continuum background is rejected while losing only 20% of the signal.

To reduce contamination from other  $B\bar{B}$  decays the quantity  $\Delta E$  – defined as the difference between the reconstructed energy and the beam energy – is required to lie within  $\pm 2.5\sigma_{\Delta E}$  from 0.0. Since  $\sigma_{\Delta E}$  is less than a pion mass, – 15 to 45 MeV/c<sup>2</sup> – this cut is very effective in reducing the background contribution from misreconstructed  $B$  decays which differ by one or more pions.

The number of fully reconstructed  $B$  in each mode is determined by fitting the beam-constrained mass to a single Gaussian plus a background shape. The beam-constrained mass variable is defined as the usual invariant mass but with the energy of the  $B$  replace by the beam energy. The beam-constrained mass distributions for 12 decay modes, separated into  $B^0$  and  $B^-$  modes, are shown in Fig. 3. These decay modes are color-allowed, that is, they can proceed by the external spectator diagram. The measured branching fractions are listed in Table 1.

CLEO II has also searched for color-suppressed decays to a single charmed meson,  $B^0 \rightarrow D^{(*)0}X^0$ . So far no clear signal has been observed. The analysis presented in Ref. [10] uses the full reconstruction technique but the signal extraction is done using the  $\Delta E$  variable instead of the beam-constrained mass

Table 2: Limits on Branching Fractions for  $\bar{B}^0 \rightarrow D^{(*)0}(n\pi)^0$  Decay Modes <sup>23</sup>

Class II Decays @ 90% C.L.			
Mode	$\mathcal{B}r$ (%)	Mode	$\mathcal{B}r$ (%)
$D^0\pi^0$	$< 0.01$	$D^{*0}\pi^0$	$< 0.04$
$D^0\eta$	$< 0.01$	$D^{*0}\eta$	$< 0.02$
$D^0\eta'$	$< 0.10$	$D^{*0}\eta'$	$< 0.16$
$D^0\rho^0$	$< 0.04$	$D^{*0}\rho^0$	$< 0.06$
$D^0\omega$	$< 0.05$	$D^{*0}\omega$	$< 0.08$

technique. The 90% C.L. upper limits are listed in Table 2. They are updated results obtained with the complete CLEO II data sample and replace previous CLEO II numbers.

### 3.2 Partial Reconstruction of $B \rightarrow D^{(*)}\pi^-$ decays at CLEO

CLEO II has recently measured the  $\bar{B}^0 \rightarrow D^{*+}\pi^-$  and  $B^- \rightarrow D^{*0}\pi^-$  branching fraction using the partial reconstruction technique <sup>14</sup>. In this method the kinematics of  $B\bar{B}$  production at the  $\Upsilon(4S)$  are exploited to fully reconstruct the decay using only the 4-momentum of the fast pion ( $\pi_f$ ) from the decay of the  $B$  meson and the slow pion ( $\pi_s$ ) from the  $D^*$  decay. The advantage of this method lies in the large increase in statistical power since the explicit reconstruction of the  $D$  meson is no longer needed. The trade-off comes in the larger backgrounds and hence greater difficulty in signal extraction.

The two pion 4-momenta together with inputs of the known masses, the  $D$ ,  $D^*$  and  $B$  meson masses, and requiring that the energy of the  $B$  be equal to the beam energy provide sufficient constraints to solve for the unknown  $D^*$  and  $D^0$  momentum. Also, energy-momentum conservation in the decay of the  $B$  meson restricts the  $D^*$  momentum vector to lie in a cone around the  $\pi_f$ . Similarly, for the  $D^*$  decay, the  $D^*$  momentum vector must lie in a cone around the  $\pi_s$ . For the two pions to be consistent with  $B \rightarrow D^*\pi$  decay the cones must overlap. This condition is required as part of the event selection criteria.

Signal extraction in this analysis is performed by inspecting the distributions of the  $\cos(\Theta_{D^*})$  and  $\cos(\Theta_B)$  where  $\Theta_{D^*}$  is defined as the angle between the  $\pi_s$  and the direction of  $D^*$  in the  $D^*$  rest frame. Similarly  $\Theta_B$  is the angle between the  $\pi_f$  and direction of the  $B$  in the  $B$  rest frame. Since the  $B$  meson is a pseudo-scalar its decay is isotropic. We thus expect the  $\cos(\Theta_B)$  distribution to be flat for signal. Since the  $D^*$  is longitudinally polarized along its direction of travel when measured from its rest frame we expect the  $\cos(\Theta_{D^*})$  distribution to be distributed as  $\cos^2 \Theta_{D^*}$  in signal.

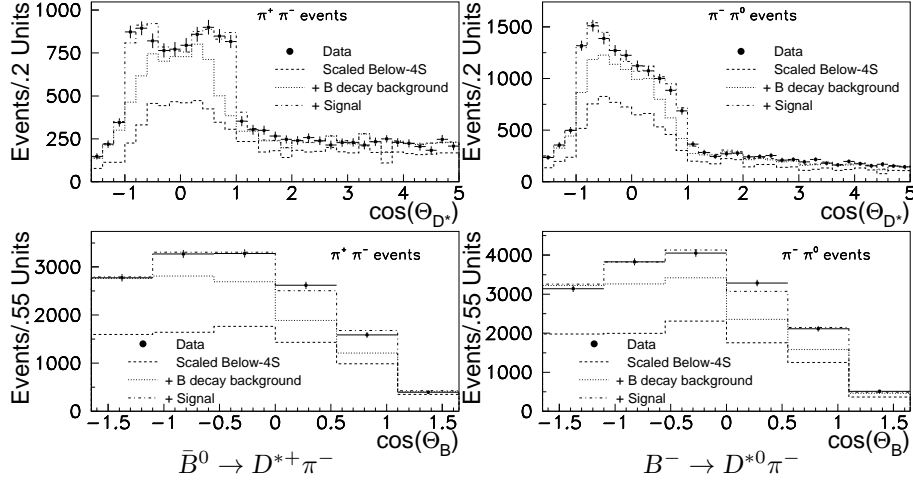


Figure 4: Projections of 2-D fit to data for the variables  $\cos(\Theta_B)$  and  $\cos(\Theta_{D^*})$ . The two figures on the left represent  $\bar{B}^0 \rightarrow D^{*+}\pi^-$  decays the two on the right are for  $B^- \rightarrow D^{*0}\pi^-$  decays. The population of events in the non-physical region  $|\cos(\Theta)| > 1.0$  is from mismeasured track combinations.

Figure 4 shows projections of a 2-dimensional  $\chi^2$  fit to the data. The fitting function consists of shapes for signal, continuum and  $B\bar{B}$  background. The signal and  $B\bar{B}$  background components were determined from Monte Carlo simulations while the continuum shape was modeled by off-resonance data. The overall normalization of the  $B\bar{B}$  background component is allowed to vary in the fit while the continuum component is fixed. The fitting function used in the  $\pi_f^- \pi^0$  fit contains an additional component to accommodate the contribution of the  $\bar{B}^0 \rightarrow D^{*+}\pi^-$  decay where the  $D^{*+}$  decays to  $D^+\pi^0$ . This is fixed by the  $\bar{B}^0 \rightarrow D^{*+}\pi^-$  branching fraction determined in the  $\pi_f^- \pi_s^+$  fit. The measured branching fractions are:

$$\begin{aligned} \mathcal{B}(\bar{B}^0 \rightarrow D^{*+}\pi^-) &= (2.81 \pm 0.11 \pm 0.21 \pm 0.05) \times 10^{-3} \\ \mathcal{B}(B^- \rightarrow D^{*0}\pi^-) &= (4.34 \pm 0.33 \pm 0.34 \pm 0.18) \times 10^{-3} \end{aligned}$$

where the first error is statistical the second is systematic and the third is due to the uncertainty in the  $D^*$  branching fractions. These results are in excellent agreement with the results obtained by the full reconstruction technique.

### 3.3 $B \rightarrow D_J^0(n\pi)^-$ decays

The full and partial reconstruction techniques have been used by both CLEO and ARGUS to reconstruct decays of the  $B$  meson to excited  $L = 1$  charmed



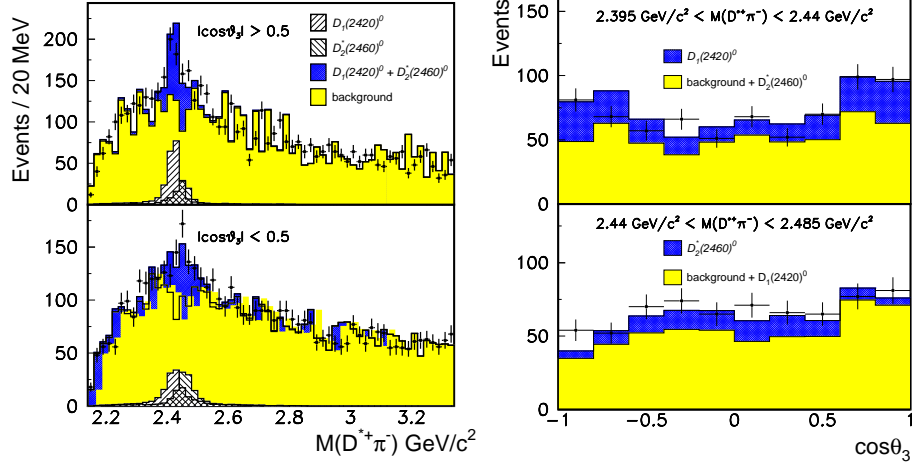


Figure 5: Projections of 2-D fit to data for the variables  $\cos\theta_3$  and  $m_{D^{*+}\pi^-}$ . The two figures on the left show the  $m_{D^{*+}\pi^-}$  in different regions of the  $\cos\theta_3$ . The figures on the right show the projection of  $\cos(\theta_3)$  in different regions of  $m_{D^{*+}\pi^-}$ . The data are the points with error bars.

mesons. Published results exist only for the  $B^- \rightarrow D_1^0(2420)\pi^-$  mode. For the  $B^- \rightarrow D_J^0\rho^-$  mode upper limits from CLEO II <sup>15</sup> are available for the  $B^- \rightarrow D_2^*(2460)^0\rho^-$  and  $B^- \rightarrow D_1(2420)^0\rho^-$  decays and from ARGUS a measurement of the sum over all  $D_J^0$  has been reported <sup>7</sup>.

There are four excited states  $D_J^{(*)}$  mesons with in a  $L = 1$  orbital angular momentum state. Two, the  $D_2^*(2460)$  and the  $D_1(2420)$  are narrow resonances which have been seen and their decays measured <sup>7</sup>. Angular momentum and parity conservation place restrictions on the strong decay of these states. The  $D_2^*(2460)$  can decay via D-wave to either  $D\pi$  or  $D^*\pi$  while the  $D_1(2420)$  can decay to  $D^*\pi$  via S-wave or D-wave.

Recently, CLEO II has reported new measurements on the  $D_1(2420)^0\pi^-$  and  $D_2^*(2460)^0\pi^-$  <sup>17</sup> using a partial reconstruction technique. The analysis follows the procedure outlined in Section 3.2. Once again the reconstruction of the decay depends on knowing the masses of the decay products, the beam-energy and the 4-momenta of the three pions,  $\pi_1, \pi_2, \pi_3$  produced in the decay chain  $B \rightarrow D_J^0\pi_1, D_J^0 \rightarrow D^{*+}\pi_2^-$  and  $D^* \rightarrow D^+\pi_3$ . In this analysis the mass of the  $D^{*+}\pi^-$  combination and the helicity angular distribution  $\cos\theta_3$  are used to identify the signal. The variable  $\theta_3$  is defined as the angle between the  $D^0$  and the direction of the  $D^*$  in the  $D^*$  rest frame and describes the helicity

Table 3: Branching Fractions for  $B \rightarrow D^{(*)}D_s^{*+}$  Decay Modes<sup>9,23</sup>

Mode	$\mathcal{Br}$ (%)	Mode	$\mathcal{Br}$ (%)
$D^+D_s^-$	$0.87 \pm 0.24 \pm 0.22$	$D^0D_s^-$	$1.18 \pm 0.21 \pm 0.27$
$D^+D_s^{*-}$	$1.00 \pm 0.35 \pm 0.25$	$D^0D_s^{*-}$	$0.82 \pm 0.25 \pm 0.19$
$D^{*+}D_s^-$	$0.87 \pm 0.22 \pm 0.18$	$D^{*0}D_s^-$	$1.32 \pm 0.40 \pm 0.37$
$D^{*+}D_s^{*-}$	$1.91 \pm 0.47 \pm 0.41$	$D^{*0}D_s^{*-}$	$2.91 \pm 0.83 \pm 0.70$

angular distribution of the  $D^*$  in the decay chain  $D_J \rightarrow D^*\pi_2, D^* \rightarrow D\pi_3$ . From angular momentum conservation in  $B \rightarrow D_2^*(2460)\pi$  we expect that the  $\cos\theta_3$  distribution to be proportional to  $\sin^2\theta_3$  while in  $B \rightarrow D_1(2420)\pi$  we expect the distribution to be proportional to  $1 + 3\cos^2\theta_3$ <sup>17</sup>.

Figure 5 shows the projections of 2-dimensional unbinned likelihood fits to the data. The two figures on the left show the projection onto the  $m_{D^{*+}\pi^-}$  axis in different regions of  $\cos\theta_3$  where either the  $D_1(2420)$  or the  $D_2^*(2460)$  are expected to dominate. The long flat tails in the signal shape result from combinations where a random track has faked a real  $\pi_2$ . The two plots on the right show the projection of fit on the  $\cos\theta_3$  distribution. Here too, the regions where either the  $D_1(2420)$  or  $D_2^*(2460)$  are expected to dominate are separated by  $m_{D^{*+}\pi^-}$  cuts. The signal and  $B\bar{B}$  background shapes were determined from Monte Carlo simulations. The continuum component was modeled in real data taken below the  $\Upsilon(4S)$  peak. The measured product branching fraction are:

$$\begin{aligned} \mathcal{B}(B^- \rightarrow D_1^0\pi^-) \times \mathcal{B}(D_1^0 \rightarrow D^{*+}\pi^-) &= (7.8 \pm 1.6 \pm 1.0 \pm 0.2) \times 10^{-4} \\ \mathcal{B}(B^- \rightarrow D_2^{*0}\pi^-) \times \mathcal{B}(D_2^{*0} \rightarrow D^{*+}\pi^-) &= (4.2 \pm 1.6 \pm 0.6 \pm 0.1) \times 10^{-4} \end{aligned}$$

The branching fraction for the individual  $B$  decays are listed in Table 1 where the authors have used isospin conservation and the measured branching fraction of  $D_2^{*0}(2460) \rightarrow D^+\pi^-$ <sup>18</sup> to deduce the following  $D_J$  decay rates

$$\mathcal{Br}(D_1(2420)^0 \rightarrow D^{*+}\pi^-) = 2/3 \text{ and } \mathcal{Br}(D_2^*(2460) \rightarrow D^{*+}\pi^-) = 0.20$$

The authors have neglected multi-pion decays to obtain these branching fractions.

### 3.4 $B \rightarrow D^{(*)}D_s^{(*)}$ decays

Another important class of two-body decays are the decays to two charmed mesons. The Cabbibo allowed process produces either a  $D_s^{*+}$  or a  $D_s^+$  and can proceed only via the external spectator diagram. The large mass of the  $D^{(*)}D_s^{(*)+}$  system implies a lower momentum transfer and hence provides a

means by which to probe a different  $q^2$  region than is possible with  $D^{(*)+}(n\pi)$  decays. Measurements of  $B \rightarrow D_s^{(*)+} D^{(*)}$  rates together with measurements on the  $B \rightarrow D^{*+} \pi^-, \rho^-$  rates allow the extraction of the  $f_{D_s}$  and  $f_{D_s^*}$  decay constants<sup>1</sup>.

Both CLEO and Argus<sup>9,7</sup> have measured  $B$  decays to Cabbibo allowed double charm final states. The CLEO II analysis reconstructs all eight decay modes exclusively using several the three  $D^0$ , one  $D^+$  and several  $D_s$  sub-channel decays. Only a subset consisting of  $2.04 fb^{-1}$  of the complete CLEO II on resonance data were used for this analysis. The values listed in Table 3 are the published CLEO II values rescaled by the  $D$  and  $D^*$  branching fractions in Ref. [8].

### 3.5 $B^- \rightarrow D^0 K^-$ decays

A search for the Cabbibo suppressed decay to  $D^0 K^-$  has been performed by CLEO II<sup>19</sup>. Interference between the  $b \rightarrow \bar{c}us$  and  $b \rightarrow u\bar{c}s$  decay, which hadronize as  $B^- \rightarrow D^0 K^-$  and  $B^- \rightarrow \bar{D}^0 K^-$  respectively can be used to determine the CKM phase ( $\gamma$ )<sup>b</sup>.

The analysis procedure features a full reconstruction technique but  $\Delta E$  is used extract the event yield. For this analysis particle ID is significantly more important because of the large background from the Cabbibo allowed  $B^- \rightarrow D^0 \pi^-$  process. At CLEO, the current particle ID system cannot distinguish with great certainty pions from kaons at high momentum. For example  $K\pi$  separation at 2.2 GeV/c is less than  $2\sigma$  where  $\sigma$  is the difference between the expected and measured energy loss  $dE/dx$  due to specific ionization in the drift chamber. Fig. 6 shows the  $\Delta E$  distribution for the  $B^- \rightarrow D^0 K^-$  with  $D^0 \rightarrow K^-\pi^+, K^-\pi^+\pi^0, K^-\pi^+\pi^-\pi^+$  combinations consistent with  $B$  production. The large background from misidentified  $B^- \rightarrow D^0 \pi^-$  is seen to overwhelm the signal. The limit reported is

$$Br(B^- \rightarrow D^0 K^-) < 4.4 \times 10^{-4} @ 90\% \text{ C.L.}$$

## 4 Test of Factorization

Theoretical models<sup>1,2,3,4,5</sup> of hadronic decays of heavy mesons invoke the factorization approximation to make definite predictions on decay rates to exclusive modes. Factorization is used in order to reduce the hadronic matrix elements to products of factorized matrix elements with one describing the creation of a hadron from the vacuum and the other describing the transition

---

<sup>b</sup>This topic is discussed in greater detail in an article by D. Atwood in these proceedings.

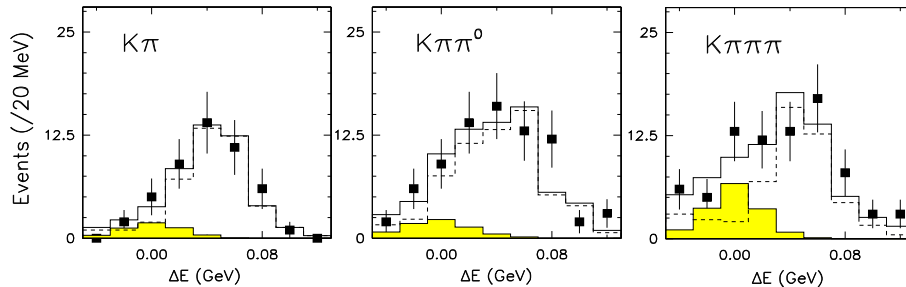


Figure 6: The distribution of the reconstructed energy minus the beam-energy for candidates that satisfy the full reconstruction selection algorithm. The data are the points, the solid hatched histogram is the signal the dashed histogram is assumed background, taken from the mass sidebands and the fit is shown by the open histogram. From left to right the  $D^0 \rightarrow K^- \pi^+$ ,  $K^- \pi^+ \pi^0$  and  $K^- 3\pi$  modes.

of the  $B$  meson. The factorized  $B \rightarrow D$  transition matrix element is equivalent to the matrix element encountered in semi-leptonic decays while the matrix element describing the creation of a meson from the vacuum is parameterized by the decay constant of the meson<sup>1</sup>.

Some theoretical motivation exists, at least for decays with large energy release, for the factorization hypothesis. These are based on “color transparency arguments” which postulate that a  $q\bar{q}$  pair created in a point-like interaction will hadronize only after a time given by its  $\gamma$  factor times a typical hadronization scale<sup>1</sup>. Thus in an energetic transition the hadronization of a light  $q\bar{q}$  pair which travels together in the same direction will not occur until it is a significant distance from the interaction region<sup>1</sup>. While this scenario describes decays such as  $B \rightarrow D^{(*)}(n\pi)^-$  where  $n\pi$  is a light meson it does not apply to  $B \rightarrow D^{(*)}D_s^{(*)}$  decays where the  $\gamma$  factors are smaller. It remains to be seen if the factorization hypothesis holds for decays that occur at lower energy transfers.

#### 4.1 Branching Fraction Tests

To test the factorization approximation we exploit the similarity between hadronic two-body decays and semi-leptonic decays. In semi-leptonic decays factorization is strictly obeyed since the leptonic current does not interact with the hadronic part. By taking the ratio of a hadronic decay rate to its semi-leptonic counterpart we can compare the experimental ratio to the theoretical expectation and thus performing a direct test of the factorization hypothesis<sup>3</sup>.

Table 4: Test of Factorization: Comparison of  $R_{\text{exp}}$  to  $R_{\text{theo}}$ <sup>21,23</sup>

$q^2$	$R_{\text{exp}}(\text{GeV}^2)$	$R_{\text{theo}}(\text{GeV}^2)$
$m_\pi^2$	$1.13 \pm 0.04 \pm 0.14$	$1.09 \pm 0.07$
$m_\rho^2$	$2.94 \pm 0.24 \pm 0.48$	$2.68 \pm 0.20$
$m_{a_1}^2$	$3.45 \pm 0.36 \pm 0.59$	$3.19 \pm 0.33$
$m_{D_s}^2$	$1.81 \pm 0.45 \pm 0.40$	$3.50(f_{D_s}/240\text{MeV})$
$m_{D_s^*}^2$	$3.76 \pm 0.93 \pm 0.84$	$3.21(f_{D_s^*}/275\text{MeV})$

If Factorization holds then

$$\frac{\mathcal{B}r(\bar{B}^0 \rightarrow D^{*+} h^-)}{\frac{d\mathcal{B}r}{dq^2}(\bar{B} \rightarrow D^* l \nu_e)|_{q^2=m_h^2}} = 6\pi^2 f_h^2 |a_1|^2 |V_{ij}|^2 X_h$$

is satisfied. The branching fraction measurements listed in Table 1 together and measurements of the semi-leptonic rate at the appropriate  $q^2$  are used. The value of the QCD parameter  $a_1$  is taken to have the strict factorization value  $a_1 = c_1(\mu) + \frac{1}{N_c} c_2(\mu) = 1.04$ , where  $c_1(\mu)$  and  $c_2(\mu)$  are the Wilson coefficients calculated at  $\mu = m_b$  and  $1/N_c = 1/3$ <sup>1</sup>. The semi-leptonic branching fraction is interpolated<sup>20</sup> from a fit to the differential branching fraction at the appropriate  $q^2$ . The  $X_h$  is a kinematic factor which depends on the masses of the hadrons and relevant form factors and is close to 1.0. Table 4 shows a comparison between the experimental and the theoretical ratios for different regions of  $q^2$ . The agreement between data and theory is quite good in the low  $q^2$  region suggesting that factorization works, at least for energetic Class I decays.

## 5 The Relative Sign and Amplitude of $a_1$ and $a_2$

Theoretical models based on the BSW approach relegate all short-distance QCD effects into QCD parameters<sup>2,3,4</sup>. In two-body tree-level decays, two parameters,  $a_1$  and  $a_2$  multiply the dominant spectator contribution from the external and internal diagrams, respectively. They provide important clues into the role played by the strong interaction. For instance, the absolute value of the QCD parameters are sensitive to the factorization scale and additional long-distance contribution<sup>1</sup>. The latter being particularly true for the  $a_2$  since it involves the difference between two small numbers. Also, the relative sign of  $a_1$  and  $a_2$  identifies the kind of interference between the internal and external spectator diagrams.

To determine the values of  $a_1$  and  $a_2/a_1$  we use the branching fraction measurements in Table 1 and 3 together with the theoretical predictions from the Neubert *et al.* model calculations<sup>3,1</sup>. Since the QCD parameters are expected to be process independent<sup>1</sup>, at least for decays that occur at similar momentum scales, we perform a least squares fit to four of the  $D^{(*)}(n\pi)$  decays, and a separate fit to the  $D^{(*)}D_s^{(*)+}$  decays. The results are:

$$\begin{aligned} |a_1|_{Dn\pi} &= 1.03 \pm 0.02 \pm 0.04 \pm 0.05 \\ |a_1|_{DD_s} &= 1.01 \pm 0.05 \pm 0.12 \pm 0.05 \end{aligned}$$

where the first error is statistical, the second is the systematic error<sup>c</sup> and the third is the error due to the uncertainty in the  $B$  lifetime/production ratio<sup>16</sup>. Consistent results are obtained using the Deandrea *et al.* model and the Neubert and Stech “New Model” in Ref. [1]. No process dependency is observed in the data.

To determine the value and the relative sign  $a_2/a_1$  we form ratios of Class III to Class I branching fractions; again using the Neubert *et al.* model calculations to extract the value from a least squares fit to data. The value obtained from the fit was:

$$\frac{a_2}{a_1} = +0.21 \pm 0.03 \pm 0.03 \mp_{0.12}^{0.13}$$

The lifetime-production fraction is taken to be 1.0 in both the fit to  $a_1$  and  $a_2/a_1$ . This is consistent with the CLEO II measurement<sup>16</sup>  $\frac{f_+ \tau_+}{f_0 \tau_0} = 1.14 \pm 0.14 \pm 0.13$ .

The positive sign for  $a_2/a_1$  suggests that the internal and external decay amplitudes interfere constructively. This is in contrast to the situation in  $D$  decay where a negative sign implies destructive interference. The destructive interference in  $D$  decays is responsible for the longer lifetime of the charged  $D$  mesons which can proceed only through the external diagram. The positive sign of  $a_2/a_1$  seems to suggest a shorter lifetime for the charged  $B$  which is not observed in data. One possible explanation for this may be that constructive interference is only found in low multiplicity  $B$  decays which constitute a small fraction of the total hadronic width. It remains to be seen if this pattern persists for other  $B$  decays.

## 6 Conclusions

Significant improvements in the precision of branching fraction measurements of exclusive hadronic  $B$  decays have been made in the recent past. This is

<sup>c</sup>The first systematic error of the  $|a_1|_{DD_s}$  is computed assuming all systematic errors except the error from the  $\mathcal{B}r(D_s^+ \rightarrow \phi\pi^+)$ , are independent in the fit. This error is a common systematic and is thus added in quadrature.

primarily due to the ever increasing statistics, particularly at  $B\bar{B}$  threshold machines, and improvements in the analysis procedure. From these precise measurement we are now able to more accurately test theoretical predictions based on factorization. We showed in Table 4 a comparison between the experimental results and theoretical predictions based on factorization. We find that in energetic Class I transition the factorization hypothesis seems to be well supported by the data. It remains to be seen if factorization holds in the higher  $q^2$  region and of the color-suppressed  $D^{(*)0}n\pi$  decays. So far none of these color-suppressed decays have been observed. Also, the QCD parameters  $a_1$  and the  $a_2/a_1$  have been determined by fitting the data to model calculations. In Class III the relative sign of  $a_2/a_1$  was found to be positive indicating that the interference between internal and external decays diagrams is constructive. This fact provides additional insight into differences between the  $D$  and  $B$  decays which occur at different factorization scales.

## 7 Acknowledgments

I would like to thank those who participated or contributed to these analyses, in particular the CLEO II, and OPAL collaborations. I would also like to take this opportunity to thank Tom E. Browder and Sandip Pakvasa and their staff for organizing an excellent Conference with a stimulating scientific program.

## References

- [1] M. Neubert and B. Stech, CERN preprint, CERN-TH/97-99, hep-ph/9705292, to appear in the Second Edition of Heavy Flavours by A.J. Buras and M. Linder (World Scientific)
- [2] M. Bauer, B. Stech and M. Wirbel, Z. Phys. **C29**, 639 (1985).
- [3] M. Neubert, V. Rieckert, B. Stech and Q. P. Xu in *Heavy Flavours* edited by A. J. Buras and H. Lindner, World Scientific, Singapore (1992).
- [4] A. Deandrea, N. Di Bartolomeo, R. Gatto and G. Nardulli, *Phys. Lett. B* **318**, 549 (1993).
- [5] C. Reader and N. Isgur, *Phys. Rev. D* **47**, 1007 (1993)
- [6] OPAL Collaboration, R. Akers *Phys. Rev. Lett.* **B337**, 196 (1994).
- [7] Review of Particle Properties, *Phys. Rev. D* **54**, (1996).
- [8] B. Barish, CLEO Collaboration, EPS Conference submission, EPS-339, CLEO CONF97-01 (1997). In this paper ratios of  $D$  branching fractions were scaled by the  $\mathcal{B}r(D^0 \rightarrow K^-\pi^+) = 0.0391 \pm 0.0008 \pm 0.0017$
- [9] T. Bergfeld *et al.*, CLEO Collaboration, *Phys. Rev. D* **53**, 4734 (1996). In this paper ratios of the  $D_s$  branching fractions were scaled by  $\mathcal{B}r(D_s^+ \rightarrow \phi\pi^+) = 0.035 \pm 0.004$ .

- [10] D.W. Bliss, CLEO Collaboration, EPS Conference submission, EPS-338, CLEO CONF97-12 (1997).
- [11] This numbers represents a weighted average of recent CLEO II results obtained from the full and partial reconstruction analyses described in Refs. [8] and [14]. Since the measurement were conducted on the same experiment some of the systematic errors are correlated. In averaging the results these correlations were taken into account using the error matrix.
- [12] The non-resonant  $\pi^0\pi^-$  component in  $D^{(*)}\rho^-$  is small. It ranges from less than 2.5% to 9.0% depending on the mode. For these modes we neglect non-resonant contributions. This analysis was performed in reference <sup>15</sup> on approximately 1/3 of the current data sample.
- [13] The non-resonant  $\pi\pi\pi$  and  $\pi\rho^0$  component in  $D^{(*)}a_1^-$  was found to be less than 12% and 24% in  $D^0a_1$  and  $D^+a_1$  decays at the 90% Confidence Level <sup>22</sup>. The event yields were corrected accordingly for the  $D^{(+,0)}a_1^-$  modes. In  $D^*a_1$  the contributions from non-resonant  $\pi^-\rho^0$  and  $D^{**}\rho$  were found to be less 9.4% and 10.6% respectively at the 90% confidence level <sup>15</sup>. We thus neglect non-resonant contributions to both  $D^{*(+,0)}a_1^-$  modes.
- [14] G. Brandenburg *et al.*, CLEO Collaboration, submitted to PRL, hep-ex/9706019
- [15] M. S. Alam *et al.*, CLEO Collaboration, *Phys. Rev. D* **50**, 43 (1994).
- [16] B. Barish *et al.*, CLEO Collaboration, *Phys. Rev. D* **51**, 1014 (1995).
- [17] J. Gronberg *et al.*, CLEO Collaboration, ICHEP96 Conference submission, PA05-69, CLEO CONF96-25, (1996)
- [18] L. Montanet *et al.*, *Phys. Rev. D* **50**, 1173 (1994)
- [19] J.P. Alexander *et al.*, CLEO Collaboration, ICHEP96 Conference submission, PA05-68, CLEO CONF96-27, (1996)
- [20] T.E. Browder, K. Honscheid, D. Pedrini, *Prog. Part. Nucl. Phys.* **35**, 81 (1995)
- [21] I use the following decay constant and CKM matrix element inputs to determine the  $R_{th}$  ratios. For  $f_\pi = 134 \pm 1\text{MeV}$ ,  $f_\rho = 210 \pm 5\text{MeV}$ ,  $V_{ud} = 0.975 \pm 0.001$ ,  $V_{cs} = 0.974 \pm 0.001$ .
- [22] J. L. Rodriguez, University of Florida Dissertation (1995).
- [23] The difference in the values listed and the numbers reported at the conference are due to recent CLEO II updates and a rescaling of previous results to  $D$  and  $D^*$  branching fraction used in Ref. [8]. These numbers were not yet available in March 1996.